

FlowFeat: Pixel-Dense Embedding of Motion Profiles

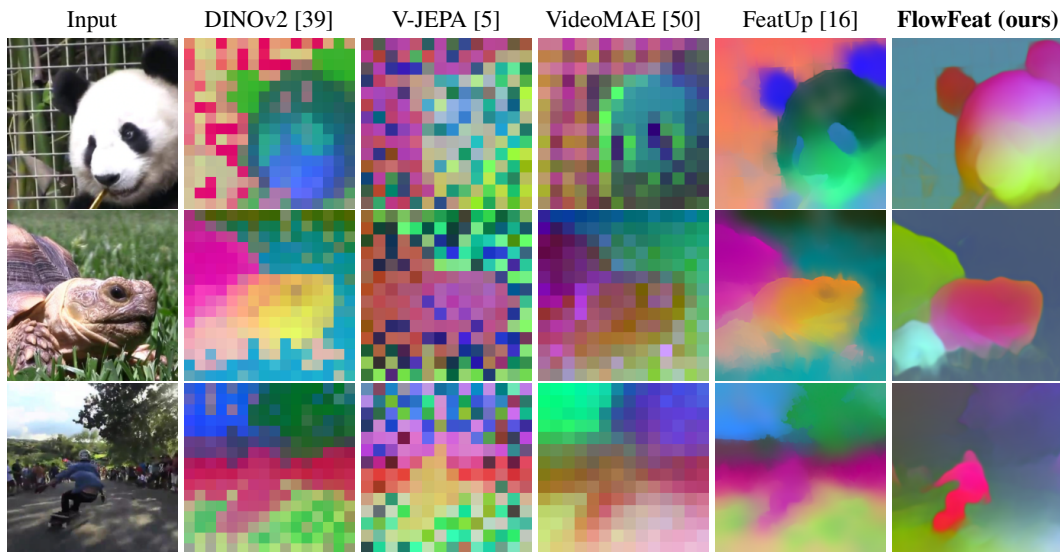
Nikita Araslanov^{1,2}Anna Sonnweber¹Daniel Cremers^{1,2}¹TU Munich ²MCML

Figure 1: **FlowFeat** is a versatile feature representation at pixel-level resolution. Embedding profiles of plausible motion, FlowFeat stands out from existing techniques by offering excellent spatial precision coupled with temporal consistency. Here, we visualise (using PCA with three principal components) a comparison of FlowFeat with the feature maps of the state-of-the-art vision encoders.

Abstract

Dense and versatile image representations underpin the success of virtually all computer vision applications. However, state-of-the-art networks, such as transformers, produce low-resolution feature grids, which are suboptimal for dense prediction tasks. To address this limitation, we present FlowFeat, a high-resolution and multi-task feature representation. The key ingredient behind FlowFeat is a novel distillation technique that embeds a distribution of plausible apparent motions, or *motion profiles*. By leveraging optical flow networks and diverse video data, we develop an effective self-supervised training framework that statistically approximates the apparent motion. With its remarkable level of spatial detail, FlowFeat encodes a compelling degree of geometric and semantic cues while exhibiting high temporal consistency. Empirically, FlowFeat significantly enhances the representational power of five state-of-the-art encoders and alternative upsampling strategies across three dense tasks: video object segmentation, monocular depth estimation and semantic segmentation. Training FlowFeat is computationally inexpensive and robust to inaccurate flow estimation, remaining highly effective even when using unsupervised flow networks. Our work takes a step forward towards reliable and versatile dense image representations.

Project website: <https://tum-vision.github.io/flowfeat>.

Code and pre-trained models (Apache-2.0 License): <https://github.com/tum-vision/flowfeat>.

1 Introduction

The feature maps of state-of-the-art self-supervised encoders (*e.g.* [9, 19]) have drastically downsampled spatial resolutions (*e.g.* by a factor of 16), as illustrated in Fig. 1. While such downsampling improves the computational efficiency of deep networks, it compromises on the accuracy of dense prediction tasks, where spatial detail is crucial. Upsampling techniques, such as those based on bilateral filters [16], can recover feature detail to an impressive degree. However, bilateral upsampling incurs a tangible computational cost and struggles under challenging illumination scenarios (*cf.* Fig. 1, third row). Alternatively, one could equip encoders with a lightweight decoder module, such as DPT [43]. However, training such decoders without human annotation is highly non-trivial. Building on this motivation, we present *FlowFeat*, a multi-task pixel-level image representation obtained in a label-efficient (or even label-free) manner.

Different from much of the existing work on representation learning, FlowFeat derives from dense motion patterns rather than the static appearance alone [3, 10, 19, 39]. While FlowFeat is a monocular model operating on a *single* input image at test time, it uses unlabelled videos for training to embed motion patterns into a pixel-level representation. Motion patterns are foundational to visual perception [35]; they encode the compositional nature of visual scenes, encompassing both semantically and geometrically meaningful phenomena. However, as Fig. 1 illustrates, video-based learning still fails to provide representations that are dense, versatile and effective [5, 14, 22].

As a step forward, we synergise state-of-the-art optical flow networks and real-world video data. On the one hand, modern optical flow networks produce dense motion estimates with outstanding accuracy, even in challenging settings [47, 49, 54]. On the other hand, datasets of casual videos provide a treasure trove of motion and scene diversity [24, 56]. Combining both ingredients in a joint learning framework, FlowFeat requires no manual annotation. Optical flow networks train predominantly on synthetically generated labels or even with self-supervision [37, 46]; video datasets derive from real-world benchmarks and require minimal curation (*e.g.* montage filtering). The key technical challenge is distilling the apparent motion in a fashion accommodating its stochastic nature.

FlowFeat addresses this challenge with a simple idea. We estimate the feature representation with a *distribution* of linear transformations. Intuitively, for a given image and a flow estimate w.r.t. a randomly sampled counterpart, FlowFeat is trained to admit a linear transformation approximating the flow. Specifically, every training iteration estimates a *lower bound* of this transformation *on-the-fly* using a least-squares formulation. The statistical nature of this lower-bound approximation (due to sampling of the image pair) accommodates motion stochasticity and proves crucial for dealing with inaccurate flow and occasional static scenes. Consequently, the distribution of linear transformations allows FlowFeat to embed a distribution of plausible motion, or *motion profiles* [44].

Overall, our work presents two contributions. First, we develop an effective self-supervised training framework that exploits the synergetic power of flow networks and large video datasets to embed motion profiles. Our framework is efficient at training time and can run comfortably within academic infrastructures. Second, we extensively evaluate the learned representation, FlowFeat, on three diverse tasks of dense prediction: video object segmentation (VOS), monocular depth estimation and semantic segmentation. Our analyses reveal a consistent benefit of FlowFeat across all tasks, exhibiting a compelling degree of temporal consistency and spatial detail. Furthermore, FlowFeat has appealing practical properties: (*i*) it is runtime- and label-efficient; (*ii*) it scales well with varying input resolution without the need for model fine-tuning, and (*iii*) it facilitates simple post-processing tasks, enhancing the quality of dense predictions without additional training.

2 Related Work

A substantial effort towards unsupervised feature representations has focused on learning from large image sets [3, 11, 17]. This development spans multiple axes of pursuit, such as model efficiency [9, 57], scalability [19, 39] and framework architecture [12]. Although pre-training from image sets dominates the research landscape in unsupervised learning, there have been natural extensions of image-based frameworks to learning from video data [5, 14, 50]. However, it remains challenging to obtain *spatio-temporal* representations that are both dense (*i.e.* pixel-level) and temporally consistent [2, 10, 53]. Central to learning spatio-temporal representations is the design of the pre-text task. One prominent technique is *cycle consistency* [22, 28, 45, 53]. It constructs a temporal palindrome

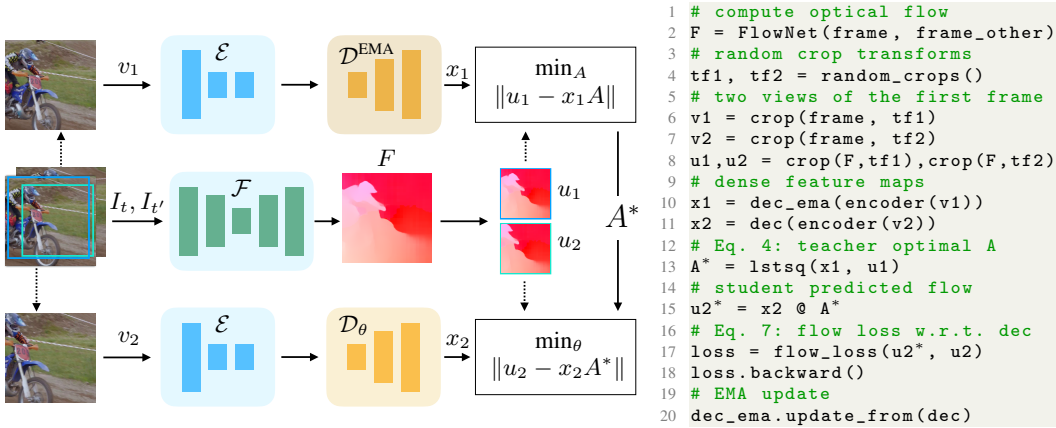


Figure 2: **Embedding motion profiles:** FlowFeat relies on the exponentially moving average (EMA) teacher model and learns to reconstruct apparent motion with a distribution of linear transformations. For a given frame I_t , we randomly sample its temporal counterpart $I_{t'}$. A pre-trained network \mathcal{F} computes optical flow $F_{(t \rightarrow t')}$. We generate two overlapping random crops of frame I_t and feed the resulting views v_1 and v_2 to the teacher and the student networks, respectively. Obtaining the optimal linear transform A^* on-the-fly with ridge regression in the teacher branch, we compute the reconstruction loss w.r.t. the flow crop u_2 to update the student parameters θ with gradient descent.

from a video sequence, ensuring consistency of a putative state in a forward and backward directions. Contrastive learning underpins another broad category of the research effort [41]. The main ideas are: constructing a reliable set of positive and negative samples [23]; combining learning on pixel, frame, and video levels [52, 55]; or jointly representing a video clip with a limited set of contrastive anchors [2]. Unlike these feature-based techniques, which have limited resolution, photometric-based learning, such as colourisation, relies on natural radiance-based appearance [51]. Lai et al. [29] leverage this technique in video-based learning, reconstructing the target frame from previous frames observed in the CIELAB colour space.

Feature upsampling strategies, such as FeatUp [16] and LoftUp [21] are closely related to our work. In contrast to bilateral upsampling [16, 27], FlowFeat is more computationally efficient and has *complementary* properties to the low-resolution encoder features. Unlike contemporaneous work [21] leveraging SAM [26], FlowFeat is label-efficient and can be trained in an unsupervised manner.

Representation learning by or with motion estimation is not new [18, 34, 40] and traces back to the earlier works on trajectory clustering and motion-based segmentation [7, 15, 31, 58]. Training FlowFeat is efficient, since it does not require pairwise sampling [34]; nor does it require object discovery [20, 40]. Instead, FlowFeat learns directly from optical flow provided from off-the-shelf networks with a distribution of linear transformations. This approach takes primary inspiration from motion profiles, which model a distribution of velocities at a given pixel [44]. *Embedding* motion profiles, FlowFeat enhances downstream accuracy of the baseline representation across diverse tasks.

3 Embedding Motion Profiles

Linear maps for optical flow. To obtain pixel-level features enhancing the low-resolution representation of pre-trained encoders, we estimate apparent motion in real-world video sequences. Off-the-shelf optical flow models exhibit exceptional generalisation, despite being trained on synthetic scenes [49, 54] or even with self-supervision [46]. However, distilling motion estimates into a *monocular* model (in contrast to previous work [32]), is highly non-trivial due to motion stochasticity.¹ Overcoming this issue, we train an image representation $\mathcal{H}_\theta(I) = x$ such that for *any* temporally neighbouring frame of I , there exists a linear operator on x which approximates the optical flow w.r.t. that neighbour. Since we estimate the linear operator uniquely for each frame neighbour, the learned

¹Naïvely approximating optical flow with a single linear layer unsurprisingly fails, as we verify in Sec. 4.4.

representation x would embed *statistical motion patterns* for each input image I – an idea inspired by motion profiles [44].

Given image I_t and its temporal neighbour $I_{t'}$ of resolution $H \times W (= N)$, we formulate the idea above with the following flow reconstruction objective (where $\|\cdot\|$ denotes an “entry-wise” norm):

$$\min_{\theta, A} \mathbb{E}_{I_t, I_{t'}} [\|\mathcal{F}(I_t, I_{t'}) - \mathcal{H}_\theta(I_t)A\|], \quad (1)$$

where $\mathcal{F}(I_t, I_{t'}) \in \mathbb{R}^{N \times 2}$ is the optical flow from a pre-trained network [49, 54]; $\mathcal{H}_\theta(I_t) \in \mathbb{R}^{N \times d}$ is our learned pixel-level feature representation and $A \in \mathbb{R}^{d \times 2}$ is a linear operator. Note that since \mathcal{H}_θ and A are both unknown, Eq. (1) is an ill-posed problem due to scale ambiguity.² Therefore, we propose to compute the corresponding loss in two steps: (i) computing a lower-bound A^* with a surrogate teacher network, while keeping \mathcal{H} fixed; (ii) computing the gradient w.r.t. θ of the original network by swapping A^* into Eq. (1) as the lower-bound linear approximation.

Student-teacher framework. Fig. 2 illustrates the framework and the corresponding training algorithm. Leveraging the mean teacher as the training model [48], our network $\mathcal{H}_\theta := \mathcal{D}_\theta \circ \mathcal{E}$ comprises a fixed (pre-trained) encoder \mathcal{E} and a trained lightweight decoder \mathcal{D}_θ , which outputs a dense feature representation of dimensionality d . The teacher model \mathcal{H}^{EMA} is equivalent to \mathcal{H}_θ with the exception of the decoder \mathcal{D}^{EMA} , which is an exponential moving average of \mathcal{D}_θ .

To construct the training batch, we sample two frames, I_t and $I_{t'}$, where $I_{t'}$ could be selected from a temporal window around I_t . We first compute optical flow $\mathcal{F}(I_t, I_{t'}) \in \mathbb{R}^{N \times 2}$ with a network pre-trained on synthetic data [49, 54] or with self-supervision [46]. Generating two overlapping random crops of the first frame I_t , we feed the corresponding views v_1 and v_2 to the teacher and student models, respectively. Using the teacher output, we solve a least-squares problem:

$$A^* = \operatorname{argmin}_A \|u_1 - \mathcal{H}^{\text{EMA}}(v_1)A\|_2, \quad (2)$$

where u_1 is the crop of the optical flow corresponding to view v_1 . In practice, we solve Eq. (2) with ridge regression, which yields stable solutions in the presence of inaccurate flow estimates and improves training stability (*cf.* Sec. 4.4 for empirical results). Specifically, we solve

$$\min_A \|u_1 - \mathcal{H}^{\text{EMA}}(v_1)A\|_2 + \gamma \|A\|_2, \quad (3)$$

in each training iteration. Here, γ is a ridge hyperparameter fixed for all models. Setting $x_1 := \mathcal{H}^{\text{EMA}}(v_1)$ to simplify the notation, the closed-form solution of Eq. (3) is naturally

$$A^* = (x_1^T x_1 + \gamma I)^{-1} x_1^T u_1. \quad (4)$$

Note that the first term has the *feature* dimensions, $d \times d$, fixed to $d = 128$ in our experiments. Therefore, computing Eq. (4) has a negligible computational cost. In contrast to previous work [34], our framework remains computationally efficient regardless of the image resolution.

Fixing A^* , we now formulate the flow reconstruction loss w.r.t. the student parameters of \mathcal{H}_θ as

$$\mathcal{L}_{L_1}(u_2, v_2) = \|u_2 - \mathcal{H}_\theta(v_2)A^*\|_1. \quad (5)$$

The loss encourages the two overlapping crops of an input frame to admit the *same* linear mapping A^* from the features to optical flow, thereby promoting grouping of pixels with similar motion patterns. Note that for zero motion (*i.e.* static scenes) the solution is $A^* = 0$, which yields zero gradient for the reconstruction term, effectively discarding such training samples in the learning process. As we also verify in the ablation study (*cf.* Tab. 3), ridge regularization and the robust L_1 loss improve resilience of the framework to inaccuracies in the estimated target flow u_1 and u_2 , respectively.

Focal gradient matching. Motion boundaries in optical flow are well-known to reveal semantic and geometric scene components. Therefore, we promote flow consistency at motion boundaries with an auxiliary second-order term implementing *focal* gradient matching:

$$\mathcal{L}_{\nabla}^x(u_2, u_2^*) = (1 - e^{-\nabla_x u_2 / \sigma}) \|\nabla_x u_2 - \nabla_x u_2^*\|_1, \quad (6)$$

where $u_2^* := \mathcal{H}_\theta(v_2)A^*$ and ∇_x is the spatial gradient along the x -axis of the image plane. Equivalently, we compute the gradient for the y -axis and the corresponding term \mathcal{L}_{∇}^y .

²If A^* and \mathcal{H}^* are the solutions, so are cA^* and \mathcal{H}^*/c for any $c \neq 0$.

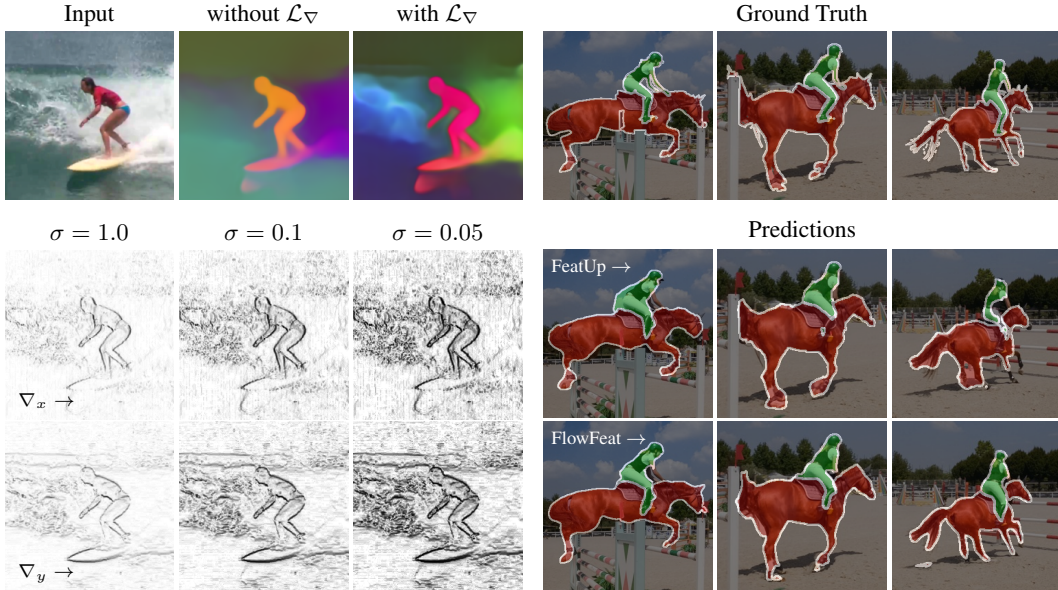


Figure 3: **Left: Focal gradient matching term \mathcal{L}_∇ .** The first row visualises the first three PCA components of FlowFeat trained with and without the gradient term. Observe sharper feature boundaries with the use of the gradient term. Additionally, we found benefit in modulating the gradient difference with a hyperparameter σ , as defined in Eq. (6). The modulation with a lower σ amplifies the effect of motion discontinuities (here, demonstrated for *image* gradients). **Right: Qualitative examples on VOS.** FlowFeat reveals finer details of the semantic masks compared to existing upsampling strategies, such as FeatUp [16].

Fig. 3 illustrates the effect of the gradient matching loss. As we also demonstrate empirically in Sec. 4.4, the gradient loss results in sharper feature maps (see the top row in Fig. 3). Note that the focal term in Eq. (6) enables modulation of the gradient loss at motion discontinuities. As the two bottom rows in Fig. 3 demonstrate, the hyperparameter σ controls the degree of this modulation: a lower value of σ results in sharper FlowFeat boundaries. However, a very low value of σ may amplify the negative effect of inaccurate flow predictions, which can also exhibit flow discontinuities.

The total second-order flow reconstruction loss is simply a weighted sum:

$$\mathcal{L}_{\text{total}} = \mathcal{L}_\nabla + \lambda \mathcal{L}_{L1}, \quad (7)$$

where \mathcal{L}_∇ is the sum of \mathcal{L}_∇^x and \mathcal{L}_∇^y , and λ is a trade-off hyperparameter kept fixed across all models.

4 Experiments

We probe FlowFeat on three diverse tasks: video object segmentation (VOS), semantic segmentation and monocular depth prediction. Our goal is to demonstrate that FlowFeat offers substantial and consistent benefits across these downstream tasks as well as across backbone models, regardless of their pre-training strategy. Overall, we train FlowFeat on top of five backbone models: Masked Autoencoder (MAE) [19] based on ViT-B16, DINO [9] based on ViT-B16 and ViT-S16, and DINO2 [39] based on ViT-B14 and ViT-S14. As the decoder architecture and the only trainable component in FlowFeat, we use the DPT model [43], which is runtime-efficient (*cf.* Tab. 7, supp. material). The flow distillation relies on SEA-RAFT [54] based on ResNet-34. However, our ablation experiments in Sec. 4.4 with the older RAFT model [49] and unsupervised flow [46] show that this choice of the flow estimator is not critical. Furthermore, Fig. 6 illustrates the resilience of the training to inaccurate flow targets. We report the results for two FlowFeat variants. FlowFeat-*YT* trains on 3471 video sequences from YouTube-VOS (CC BY 4.0, [56]). For larger backbones, we train FlowFeat-*K* on Kinetics-400 dataset (CC BY 4.0, [24]) containing 147646 videos.³ We compare our FlowFeat variants to the corresponding encoder model, as well as FeatUp [16], pre-trained on COCO-Stuff

³We exclude videos containing a montage of multiple clips to ensure temporal coherence.

Method	Train Data	Linear Probing			Local KNN		
		$\mathcal{J}\mathcal{F}$	\mathcal{J}_m	\mathcal{F}_m	$\mathcal{J}\mathcal{F}$	\mathcal{J}_m	\mathcal{F}_m
V-JEPA [5]	VideoMix2M [5]	49.0	46.1	51.9	56.7	55.6	57.8
VideoMAE [50]	Kinetics	43.3	40.9	45.8	55.1	54.6	55.6
MAE-B16 [19]	ImageNet	40.8	38.5	43.1	44.3	42.8	45.8
+ FlowFeat-K	+ Kinetics	53.8	50.1	57.5	59.1	57.3	60.8
DINO-B16 [9]	ImageNet	52.3	49.1	55.4	62.3	60.7	64.0
+ FlowFeat-YT	+ YT-VOS	55.5	52.5	58.5	64.0	62.7	65.3
+ FlowFeat-K	+ Kinetics	56.9	53.7	60.1	66.0	64.5	67.5
DINO-S16 [9]	ImageNet	49.6	46.8	52.4	61.5	59.9	63.1
+ FeatUp [16]	COCO-S	52.4	49.6	55.2	63.7	62.4	64.9
+ FlowFeat-YT	+ YT-VOS	54.1	51.1	57.0	63.7	62.0	65.5
+ FlowFeat-K	+ Kinetics	56.2	52.9	59.5	66.5	64.5	68.4
DINO2-B14 [39]	LVD*	61.6	58.5	64.7	66.4	64.4	68.5
+ FlowFeat-YT	+ YT-VOS	65.7	62.2	69.2	69.0	66.9	71.2
+ FlowFeat-K	+ Kinetics	66.1	62.3	69.9	69.9	67.7	72.1
DINO2-S14 [39]	LVD*	57.5	54.2	60.7	65.1	63.7	66.6
+ FeatUp [16]	COCO-S	60.5	57.4	63.6	65.5	65.0	66.1
+ LoftUp [21]	+ SA1B [26]	63.0	59.6	66.4	66.0	64.7	67.4
+ FlowFeat-YT	+ YT-VOS	65.8	62.0	69.7	67.6	65.6	69.6
+ FlowFeat-K	+ Kinetics	64.6	61.0	68.2	68.5	66.1	70.9

Table 1: **Video object segmentation (VOS) with linear probing and label propagation (local KNN) on DAVIS-2017 (val)**. FlowFeat significantly improves the VOS accuracy of the baselines across all tested scenarios. It further outperforms previous and concurrent upsampling techniques (FeatUp [16] and LoftUp [21]). Pre-training FlowFeat on the larger Kinetics datasets tends to produce a stronger representation. LVD* refers to the distillation from a model pre-trained on LVD [39]. LoftUp [21] uses SAM, trained with mask supervision on SA1B [26].

(CC BY 4.0 / Flickr, [8]). Recall that FeatUp stacks multiple bilateral upsamplers and preserves the feature dimensionality. For instance, FeatUp yields representations with dimensionality 384 for ViT-S, whereas FlowFeat is more compact and has a fixed dimensionality of 128 across all variants. This allows us to evaluate FlowFeat in a complementary fashion to the backbone encoding by jointly fitting a high-resolution probe on FlowFeat and a low-resolution probe on the fixed encoder.

Implementation details (see also Sec. B). Training FlowFeat is computationally inexpensive. To train one model, we use a *single* GPU with 46GB of memory. The training proceeds with mini-batches of 128 images, input resolution 224×224 and AdamW optimiser [25, 33] with learning rate 10^{-4} and no weight decay. For the hyperparameters, we empirically set $\lambda = 0.1$, $\sigma = 0.1$ and $\gamma = 1.0$ and did not observe sensitivity to moderate deviations from these values. We train FlowFeat for 500 epochs on YouTube-VOS and for 100 epochs on Kinetics. In wall-clock time with one A40 GPU, the training takes only 24 hours and 3 days for YouTube-VOS and Kinetics, respectively.

4.1 Video object segmentation

We evaluate FlowFeat on semi-supervised video object segmentation (VOS) using 30 validation sequences from DAVIS-2017 (CC BY-SA 4.0, [42]). The task is to propagate the ground-truth annotation defined in the first frame to the rest of the video. Therefore, performing well on this task would indicate the capacity for temporal invariance as well as pixel-level semantic discrimination.

Previous evaluation protocols for VOS employ a variant of a localised k-nearest neighbour classifier [2, 22, 29], referred to as *local KNN* in the following. This probing technique is known to be brittle, exhibiting high volatility w.r.t. its hyperparameters [36]. For consistency with previous work, we stick to the implementation of local KNN provided by Caron et al. [9]. However, we additionally evaluate VOS with *linear probing*, as the more established and interpretable technique in representation learning [11, 17]. Linear probing extends seamlessly to the VOS task. Specifically, for each video, we train a linear classifier using the ground-truth segmentation provided for the first frame. We apply the linear classifier to the remaining frames to obtain the segmentation result. For both probing strategies – linear probing and local KNN – we compute the mean region similarity \mathcal{J}_m , the mean contour-based accuracy \mathcal{F}_m and their mean $\mathcal{J}\mathcal{F}$. Tab. 1 reports the results. Across all pre-training methods and metrics, FlowFeat achieves a consistent and substantial improvement in VOS accuracy. The benefit is especially significant for MAE-B16, where FlowFeat improves the baseline by staggering 13.0% / 14.8% $\mathcal{J}\mathcal{F}$ with linear probing / local KNN. However, FlowFeat also surpasses stronger baselines, e.g. DINO2-B14 (+4.5% / +3.5% $\mathcal{J}\mathcal{F}$) and FeatUp (+3.8% / +2.8% $\mathcal{J}\mathcal{F}$ for DINO-S16 and +5.3% / +3.0% for DINO2-S14 $\mathcal{J}\mathcal{F}$). As illustrated in Fig. 3 (right), the improvement is especially pronounced at the object boundaries. FeatUp enhances VOS accuracy for both baselines (DINO-S16 and DINO2-S14), but these improvements are more modest. FeatUp also struggles with inputs of higher resolution, introducing static feature artefacts, see the supplemental videos and further analysis

Table 2: **Probing semantic segmentation and monocular depth.** On COCO-Stuff 2017 (val), FlowFeat advances the segmentation quality across all baselines as well. A lightweight refinement using FlowFeat++ (numbers in parentheses) further boosts the accuracy without any parameter training. On NYUv2 (val), FlowFeat significantly improves the depth accuracy across all pre-trained encoders – in contrast to FeatUp, which struggles to improve upon its baselines.

Method	Semantic Segmentation		Depth Estimation			
	mIoU \uparrow	pAcc \uparrow	RMSE \downarrow	δ_1 \uparrow	δ_2 \uparrow	δ_3 \uparrow
MAE-B16 [19]	46.0	71.5	0.4534	83.68	96.98	99.28
+ FlowFeat-K	47.2	72.9	0.4400	84.43	97.18	99.35
DINO-B16 [9]	46.1	72.0	0.4287	86.15	97.61	99.47
+ FlowFeat-K	48.2	73.7	0.4176	86.87	97.71	99.50
FeatUp – DINO-S16 [16] (++)	41.6 (42.1)	69.5 (69.9)	0.4624	83.54	96.90	99.32
DINO-S16 [9]	39.6	67.5	0.4634	83.60	96.94	99.32
+ FlowFeat-YT (++)	44.7 (45.9)	71.4 (72.5)	0.4410	85.26	97.17	99.30
+ FlowFeat-K (++)	44.2 (45.4)	71.3 (72.3)	0.4422	84.81	97.19	99.37
DINO2-B14 [39]	58.1	78.0	0.3091	94.14	99.32	99.89
+ FlowFeat-K	60.4	79.8	0.2791	95.55	99.52	99.93
FeatUp – DINO2-S14 [16] (++)	58.3 (58.5)	79.1 (79.2)	0.3207	93.29	99.18	99.86
DINO2-S14 [39]	56.2	77.3	0.3294	92.97	99.11	99.85
+ FlowFeat-YT (++)	58.0 (59.4)	78.7 (79.7)	0.3072	93.91	99.25	99.86
+ FlowFeat-K (++)	58.1 (59.6)	78.9 (79.9)	0.3061	94.12	99.31	99.88

in Tab. 6. Similarly, the contemporaneous work, LoftUp [21], achieved inferior accuracy despite the implicit leverage of vast mask supervision via SAM [26]. Video-based models, such as V-JEPA [5] and VideoMAE [50], are also remarkably ineffective.

Overall, the improvements on VOS metrics provide compelling evidence that FlowFeat encapsulates a high degree of temporal invariance and feature detail, with complementary properties to the encoder representation. Furthermore, the larger Kinetics dataset tends to produce a stronger variant of FlowFeat. This observation indicates that FlowFeat has the promising capacity to scale with the ever-increasing volume of real-world videos.

4.2 Semantic segmentation

We follow the setting of FeatUp [16] and use COCO-Stuff 2017 with $C = 27$ coarsely annotated categories [8]. Since FlowFeat focuses on motion patterns rather than global semantic alignment, it may lack consistent semantic structure across images; therefore, we employ attention probing [5] to derive image-specific class prototypes. In more detail, we define $C = 27$ learnable queries attending the FlowFeat representation with a single layer of cross-attention. We freeze the models and train the probes on 256×256 centre crops using the cross-entropy loss. Additionally, we demonstrate that FlowFeat can further boost the segmentation accuracy with a simple adaptation of a lightweight post-processing technique. Concretely, we adapt the local mask refinement strategy (PAMR) [1], but leverage FlowFeat instead of the image intensity to refine the segmentation result. Note that such a refinement is not possible by the use of the probes alone due to their feed-forward nature. We refer to this straightforward extension as FlowFeat++. Sec. B.2 provides further details.

Tab. 2 reports the mean pixel accuracy and the mean IoU. The results align with our observations in VOS experiments: FlowFeat boosts the accuracy across all baseline models. Particularly notable are the improvements w.r.t. smaller models. For example, FlowFeat surpasses DINO-S16 by 5.1% and 4.6% with FlowFeat-YT and FlowFeat-K, respectively. Without the refinement, FlowFeat performs competitively with FeatUp [16] based on DINO2-S14 and outperforms it for DINO-S16. Furthermore, the FlowFeat-based refinement significantly enhances the segmentation quality. For example, FlowFeat-K++ improves over FlowFeat-K by a notable margin of 1.5% mIoU. By contrast, FeatUp does not profit from the refinement as much.

Fig. 5 visualises the segmentation results for the DINO2-S14 backbone, with and without the refinement. Initial predictions of the probes are coarse and lack detail, especially around object boundaries. Leveraging the high-resolution FlowFeat representation (visualised with PCA), the refinement leads to sharper mask alignment with image boundaries.

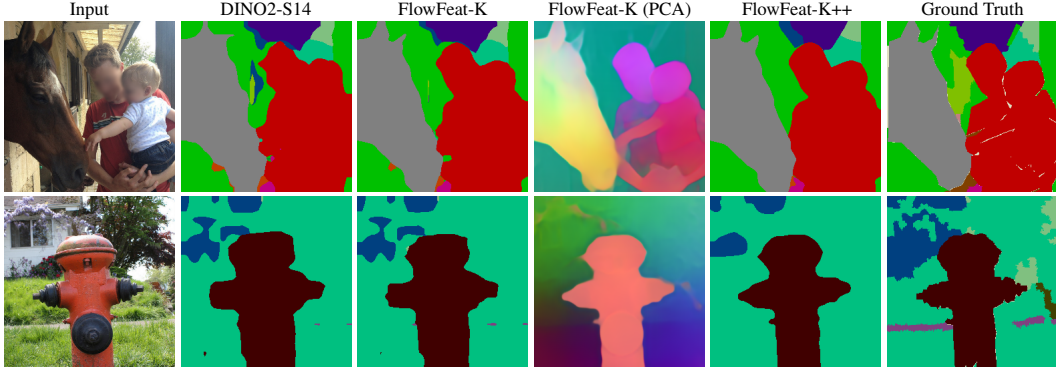


Figure 5: **Semantic segmentation and post-hoc refinement (++) with FlowFeat.** The segmentation masks from FlowFeat exhibit a high level of boundary accuracy. The FlowFeat representation, visualised with PCA, identifies prominent scene elements with a fine-grained detail. A lightweight post-hoc refinement (FlowFeat-K++), based on PAMR [1], leverages the pairwise pixel similarity embedded by FlowFeat (instead of image intensities) to improve the results further.

In summary, FlowFeat provides a significant boost also for downstream semantic tasks. The feature representation offers a high degree of spatial detail and also lends itself well to lightweight post-processing without the need for additional training.

4.3 Monocular depth estimation

We evaluate FlowFeat on a geometric task, monocular depth estimation, using NYUv2 [38], following the evaluation protocol of Banani et al. [4]. Similar to the VOS setting, we compare FlowFeat against self-supervised backbones: MAE [19], DINO [9], and DINO2 [39]. As in semantic segmentation, we use attention probing [5] to extract the depth-specific prototypes from FlowFeat. Specifically, we utilise the AdaBins [6] formulation that quantises the depth into 256 bins. The depth value is a weighted sum of the predicted distribution across the bins and the corresponding depth value of the bin. Following Banani et al. [4], we optimise the model using a weighted combination of the scale-invariant depth loss [6] and a gradient loss. Sec. B provides further details on probe implementation and training.

Adhering to the setting of Banani et al. [4], we train the probes on the NYUv2’s training set (24231 images) and evaluate the models on 480×480 centre crops of the 1449 validation images [38]. As the standard depth metrics, we report the root-mean-squared error (RMSE) and the inlier rates at three thresholds. Specifically, δ_i corresponds to the fraction of depth predictions d satisfying $\max(d/d^*, d^*/d) < 1.25^i$ w.r.t. the ground-truth d^* .

Tab. 2 summarises the quantitative results. In line with our observations on VOS and semantic segmentation, FlowFeat achieves a notable boost across all baseline models. For example, FlowFeat-K reduces RMSE w.r.t. the DINO-S16 model by 0.051 and increases the δ_1 by 3.16%. By contrast, we did not observe benefit from the high-resolution FeatUp, which appears to be biased towards the pre-training resolution of 224×224 . Notably, we did not observe such a detrimental bias in FlowFeat.

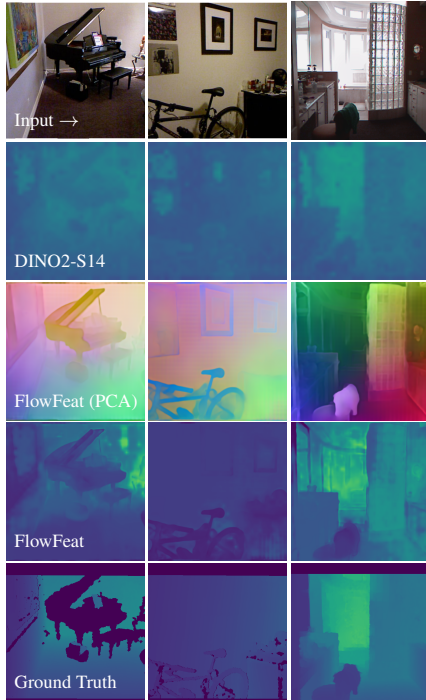


Figure 4: **Depth probing.** FlowFeat significantly improves depth estimates for challenging elements, such as non-Lambertian surfaces (e.g. left, the piano), intricate structures (e.g. middle, the bicycle), and under- and oversaturated image areas (e.g. right, a bathroom).

Table 3: **Ablation study on DAVIS-2017 (val).** Following Sec. 4.1, we perform linear probing on VOS in a set of ablation experiments. The Δ reports the absolute difference in the corresponding metric w.r.t. the baseline. The ridge regularisation in FlowFeat is crucial, but the choice of the flow estimator is not instrumental.

Baseline: DINO2-S14	$\mathcal{J}\mathcal{F} / \Delta$	\mathcal{J}_m / Δ	\mathcal{F}_m / Δ
+Random DPT	58.7	55.2	62.2
+FlowFeat-YT	65.8	62.0	69.7
(a) naïve	56.7 -9.1	52.8 -9.2	60.5 -9.2
(b) $\gamma = 0.001$, cf. Eq. (4)	58.2 -7.6	54.9 -7.1	61.5 -8.2
(c) w/o \mathcal{L}_∇ , cf. Eq. (6)	64.3 -1.5	61.0 -1.0	67.7 -2.0
(d) \mathcal{L}_{L_2}	63.3 -2.4	59.8 -2.2	67.0 -2.7
(e) w/o \mathcal{L}_{L_1} , cf. Eq. (5)	65.3 -0.5	61.6 -0.4	69.0 -0.7
(f) RAFT	65.2 -0.6	61.6 -0.4	68.8 -0.9
(g) SMURF (unsupervised)	64.1 -1.7	60.7 -1.3	67.5 -2.2
(h) temp. window $\times 2$	65.5 -0.3	62.1 +0.1	68.9 -0.8
(i) next frame only	65.8 0.0	62.2 +0.2	69.4 -0.3

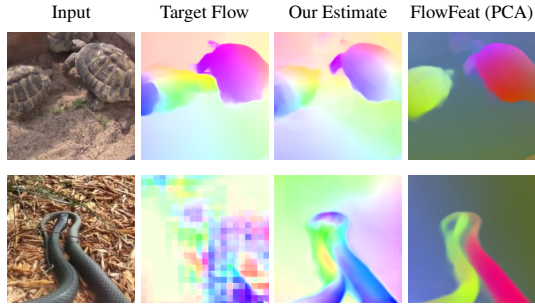


Figure 6: **Resilience to inaccurate flow targets.** Despite inaccurate and even artefact-prone predictions from optical flow networks, FlowFeat learns a reasonable flow approximation without compromising the feature representation.

We visually inspect the results in Fig. 4 for the DINO2-S14 backbone. In contrast to the low-quality depth estimates extracted from the frozen encoder, FlowFeat representation exhibits an impressive degree of fine-grained detail. This is indeed noteworthy, considering that FlowFeat originates from video data and was not trained for such static scenes. FlowFeat is also robust to under- and oversaturated image areas (cf. Fig. 4, the rightmost column) and infers highly plausible depth where the ground truth is not available due to surface specularities (cf. Fig. 4, the piano).

In summary, the results suggest that the motion profiles embedded by FlowFeat provide strong geometric cues. FlowFeat not only enhances the depth awareness across all baselines, but also scales compellingly with the increased amount of video data for pre-training: FlowFeat-K outperforms the less data-intensive FlowFeat-YT across virtually all settings and metrics.

4.4 Ablation study

We conduct an ablation study of FlowFeat on the DAVIS-2017 (val) benchmark. The study follows the evaluation protocol with linear probing from Sec. 4.1. Using ViT-S14 backbone pre-trained with DINO2 [39], we train a number of FlowFeat configurations on YouTube-VOS [56]. Tab. 3 reports the results. As a sanity check, we verify that a randomly initialised DPT decoder has virtually no effect on the VOS accuracy (cf. Tab. 3 in grey). Similarly, (a) naïvely fitting optical flow with a *single* linear layer (instead of a distribution) is futile. Next, (b) we verify the benefit of estimating the optimal operator A^* in Eq. (5) with ridge regression. To compare with the baseline setting of $\gamma = 1$ (cf. Eq. (4)), we trained the model with $\gamma = 10^{-3}$. We found the training numerically unstable with $\gamma = 0$. Thus, setting γ to 10^{-3} provides a reasonable approximation to removing the effect of L2-regularisation on the linear operator A . In this case, the VOS accuracy drastically deteriorates across all metrics, which justifies the crucial need for ridge regularization. (c) We train FlowFeat without the second-order term, \mathcal{L}_∇ in Eq. (6). A drop in the downstream accuracy (e.g. -2.0% \mathcal{F}_m) suggests that FlowFeat exploits motion boundaries in its representation, in line with the established view that motion boundaries are strong semantic cues. (d) Replacing the L_1 reconstruction loss by L_2 distance in Eq. (5) reduces $\mathcal{J}\&\mathcal{F}$ from 65.8% to 63.4%, supporting the robustness of L_1 in comparison to L_2 . Next, (e) we explore a configuration without the L1 reconstruction term by setting $\lambda := 0$ in Eq. (7). Surprisingly, the drop in accuracy is not substantial. This suggests that the training process can succeed with the gradient loss alone. However, we observed that including the L1 reconstruction term tends to improve the convergence speed consistently across all models. In the next experiments (f,g), we replace SEA-RAFT [54] with the RAFT model [49] and the unsupervised SMURF [46], respectively. The drop in the VOS accuracy is not significant, which demonstrates that obtaining FlowFeat is not sensitive to a specific choice of the flow model. Fig. 6 further examines the training resilience to inaccurate target flow. In both examples, the optical flow from the pre-trained network is inaccurate (even artefact-prone), yet it has no visible effect on the quality of FlowFeat. Curiously, the second example in Fig. 6 also reveals one limitation of FlowFeat: the apparent motion of the tail and the head of the snake have opposite directions, which decouples their feature representation.

Finally, (h,i) we test two strategies for sampling frame pairs from a video in Tab. 3. Our base configuration uses a temporal window of 5 frames and can select frame t' either from the past or the future. We increase this temporal window to 9 (h) , which leads to a slight deterioration of VOS accuracy – presumably due to the more challenging estimation of optical flow. The setting (i) selects the immediate next future frame as t' . Here, the VOS accuracy barely changes. This implies that (i) FlowFeat does not simply overfit apparent motion (compare to (a)), and (ii) the motion samples *across the dataset*, not just a temporal window, play a more critical role in embedding motion profiles.

Further study. Our further analysis, provided in the supplemental material, shows that: (1) FlowFeat scales well with the input resolution, further improving the VOS accuracy when the input resolution is doubled (*cf.* Tab. 6); (2) the accuracy gains from FlowFeat do not arise merely from higher resolution of the feature map per se, but from its complementary motion-derived properties (*cf.* Tab. 5a); (3) FlowFeat also scales effectively to larger transformer models (*e.g.* ViT-L) (*cf.* Tab. 5b).

5 Limitations

Application scope. FlowFeat relies on a pre-trained optical flow network and video data for training. It assumes either brightness constancy in the video stream or availability of synthetic data for pre-training the optical flow model. While these assumptions generally hold for standard RGB videos, they may not apply in other domains, such as medical imaging (*e.g.* MRI, CT), thermal imaging or low-light scenarios.

Frozen backbone. Recall that training FlowFeat involves updating only the decoder parameters, while keeping the encoder parameters fixed. Consequently, the encoder representation imposes an upper bound on FlowFeat’s downstream accuracy, especially in terms of high-frequency content. Although we have shown that FlowFeat generalises across widely used self-supervised encoders, such as MAE [19], DINO [9], DINOv2 [39] and across different model capacities, FlowFeat may be less effective with backbones that underrepresent high-frequency details in their intermediate feature maps.

Motion bias. Owing to its training approach, FlowFeat tends to emphasise image regions with larger magnitudes of expected motion, typically corresponding to foreground dynamic objects, relative to the static background areas. To quantitatively assess this behaviour, we report per-category IoU scores on COCO-Stuff in Tab. 4, following the probing protocol described in Sec. 4. We observe that the improvement on the “person” category is indeed more pronounced than for static classes. Nevertheless, FlowFeat yields consistent accuracy gains across all categories, regardless of whether they are static or dynamic in nature.

Model	Person	Wall	Landscape	Vegetation	Ground
DINO-S16	69.3	46.5	43.9	65.5	33.3
+ FlowFeat -YT	75.6	50.0	50.8	69.9	37.0
DINO-B16	72.9	51.4	51.0	70.3	38.9
+ FlowFeat -K	77.8	52.9	53.1	71.7	39.6
DINOv2-S14	76.9	57.6	59.2	71.0	44.6
+ FlowFeat -YT	81.7	59.3	60.5	73.0	45.7
DINOv2-B14	77.0	59.2	59.6	70.3	44.9
+ FlowFeat -K	83.0	61.7	61.3	72.3	45.1
MAE-B16	72.2	50.8	52.7	66.9	36.1
+ FlowFeat -K	78.6	51.3	53.7	69.9	38.8

Table 4: **Semantic segmentation accuracy on COCO-Stuff (IoU, %).** As expected from motion parallax, the gains on (potentially) dynamic classes (*e.g.* “person”) are larger compared to that of typical background categories (*e.g.* “vegetation”). Nevertheless, FlowFeat leads to a consistent segmentation improvement across *all* categories.

6 Conclusion

We presented FlowFeat, a pixel-dense and versatile representation embedding motion profiles. Our experiments provide compelling evidence that FlowFeat enhances the representation power of pre-trained encoders across all downstream tasks considered in our study. Specifically, FlowFeat possesses temporal consistency and exhibits a remarkable level of spatial detail, encompassing semantic and geometric cues without explicit supervision. More broadly, our work addresses motion stochasticity in a principled fashion, revealing a powerful synergy between optical flow networks and large video datasets. FlowFeat takes a significant step towards label-efficient and versatile models for high-precision tasks, such as image-based 3D reconstruction, object-level segmentation and tracking.

Acknowledgements. This work was supported by the ERC Advanced Grant SIMULACRON and DFG project CR 250/26-1 “4D-YouTube”. NA thanks Junhwa Hur and Jochen Gast for their valuable feedback.

References

- [1] N. Araslanov and S. Roth. Single-stage semantic segmentation from image labels. In *CVPR*, 2020.
- [2] N. Araslanov, S. Schaub-Meyer, and S. Roth. Dense unsupervised learning for video segmentation. In *NeurIPS*, 2021.
- [3] M. Assran, Q. Duval, I. Misra, P. Bojanowski, P. Vincent, M. G. Rabbat, Y. LeCun, and N. Ballas. Self-supervised learning from images with a joint-embedding predictive architecture. In *CVPR*, 2023.
- [4] M. E. Banani, A. Raj, K. Maninis, A. Kar, Y. Li, M. Rubinstein, D. Sun, L. J. Guibas, J. Johnson, and V. Jampani. Probing the 3D awareness of visual foundation models. In *CVPR*, 2024.
- [5] A. Bardes, Q. Garrido, J. Ponce, X. Chen, M. G. Rabbat, Y. LeCun, M. Assran, and N. Ballas. Revisiting feature prediction for learning visual representations from video. *TMLR*, 2024.
- [6] S. Bhat, I. Alhashim, and P. Wonka. AdaBins: Depth estimation using adaptive bins. *CVPR*, 2020.
- [7] T. Brox and J. Malik. Object segmentation by long term analysis of point trajectories. In *ECCV*, 2010.
- [8] H. Caesar, J. Uijlings, and V. Ferrari. COCO-Stuff: Thing and stuff classes in context. In *CVPR*, 2018.
- [9] M. Caron, H. Touvron, I. Misra, H. Jégou, J. Mairal, P. Bojanowski, and A. Joulin. Emerging properties in self-supervised vision transformers. In *ICCV*, 2021.
- [10] M. Caron, N. Houlsby, and C. Schmid. Location-aware self-supervised transformers for semantic segmentation. In *WACV*, 2024.
- [11] T. Chen, S. Kornblith, M. Norouzi, and G. E. Hinton. A simple framework for contrastive learning of visual representations. In *ICML*, 2020.
- [12] X. Chen and K. He. Exploring simple siamese representation learning. In *CVPR*, 2021.
- [13] D. Eigen, C. Puhrsch, and R. Fergus. Depth map prediction from a single image using a multi-scale deep network. In *NIPS*, 2014.
- [14] C. Feichtenhofer, H. Fan, Y. Li, and K. He. Masked autoencoders as spatiotemporal learners. In *NeurIPS*, 2022.
- [15] K. Fragkiadaki, P. Arbeláez, P. Felsen, and J. Malik. Learning to segment moving objects in videos. In *CVPR*, 2015.
- [16] S. Fu, M. Hamilton, L. E. Brandt, A. Feldman, Z. Zhang, and W. T. Freeman. FeatUp: A model-agnostic framework for features at any resolution. In *ICLR*, 2024.
- [17] J. Grill, F. Strub, F. Altché, C. Tallec, P. H. Richemond, E. Buchatskaya, C. Doersch, B. Á. Pires, Z. Guo, M. G. Azar, B. Piot, K. Kavukcuoglu, R. Munos, and M. Valko. Bootstrap your own latent – A new approach to self-supervised learning. In *NeurIPS*, 2020.
- [18] T. Han, W. Xie, and A. Zisserman. Self-supervised co-training for video representation learning. In *NeurIPS*, 2020.
- [19] K. He, X. Chen, S. Xie, Y. Li, P. Dollár, and R. B. Girshick. Masked autoencoders are scalable vision learners. In *CVPR*, 2022.
- [20] O. J. Hénaff, S. Koppula, E. Shelhamer, D. Zoran, A. Jaegle, A. Zisserman, J. Carreira, and R. Arandjelovic. Object discovery and representation networks. In *ECCV*, 2022.
- [21] H. Huang, A. Chen, V. Havrylov, A. Geiger, and D. Zhang. LoftUp: Learning a coordinate-based feature upsampler for vision foundation models. *arXiv:2504.14032 [cs.CV]*, 2025.
- [22] A. Jabri, A. Owens, and A. A. Efros. Space-time correspondence as a contrastive random walk. In *NeurIPS*, 2020.
- [23] S. Jeon, D. Min, S. Kim, and K. Sohn. Mining better samples for contrastive learning of temporal correspondence. In *CVPR*, 2021.

- [24] W. Kay, J. Carreira, K. Simonyan, B. Zhang, C. Hillier, S. Vijayanarasimhan, F. Viola, T. Green, T. Back, P. Natsev, M. Suleyman, and A. Zisserman. The Kinetics human action video dataset. *arXiv:1705.06950 [cs.CV]*, 2017.
- [25] D. P. Kingma and J. Ba. Adam: A method for stochastic optimization. In *ICLR*, 2015.
- [26] A. Kirillov, E. Mintun, N. Ravi, H. Mao, C. Rolland, L. Gustafson, T. Xiao, S. Whitehead, A. C. Berg, and W.-Y. Lo et al. Segment anything. In *CVPR*, 2023.
- [27] J. Kopf, M. F. Cohen, D. Lischinski, and M. Uyttendaele. Joint bilateral upsampling. *ACM Trans. Graph.*, 26(3):96, 2007.
- [28] Z. Lai and W. Xie. Self-supervised video representation learning for correspondence flow. In *BMVC*, 2019.
- [29] Z. Lai, E. Lu, and W. Xie. MAST: A memory-augmented self-supervised tracker. In *CVPR*, 2020.
- [30] Z. Li and N. Snavely. MegaDepth: Learning single-view depth prediction from internet photos. In *CVPR*, 2018.
- [31] C. Liu, A. Torralba, W. T. Freeman, F. Durand, and E. H. Adelson. Motion magnification. *ACM Trans. Graph.*, 24(3):519–526, 2005.
- [32] P. Liu, M. R. Lyu, I. King, and J. Xu. Learning by distillation: A self-supervised learning framework for optical flow estimation. *IEEE Trans. Pattern Anal. Mach. Intell.*, 44(9):5026–5041, 2022.
- [33] I. Loshchilov and F. Hutter. Decoupled weight decay regularization. In *ICLR*, 2019.
- [34] A. Mahendran, J. Thewlis, and A. Vedaldi. Cross pixel optical-flow similarity for self-supervised learning. In *ACCV*, 2018.
- [35] D. Marr and L. Vaina. Representation and recognition of the movements of shapes. *Proceedings of the Royal Society of London. Series B. Biological Sciences*, 214(1197):501–524, 1982.
- [36] D. McKee, Z. Zhan, B. Shuai, D. Modolo, J. Tighe, and S. Lazebnik. Transfer of representations to video label propagation: Implementation factors matter. *arXiv:2203.05553 [cs.CV]*, 2022.
- [37] S. Meister, J. Hur, and S. Roth. UnFlow: Unsupervised learning of optical flow with a bidirectional census loss. In *AAAI*, 2018.
- [38] P. K. Nathan Silberman, Derek Hoiem and R. Fergus. Indoor segmentation and support inference from rgb-d images. In *ECCV*, 2012.
- [39] M. Oquab, T. Darcet, T. Moutakanni, and H. V. et al. DINOv2: Learning robust visual features without supervision. *arXiv:2304.07193 [cs.CV]*, 2023.
- [40] D. Pathak, R. B. Girshick, P. Dollár, T. Darrell, and B. Hariharan. Learning features by watching objects move. In *CVPR*, 2017.
- [41] P. O. Pinheiro, A. Almahairi, R. Y. Benmalek, F. Golemo, and A. C. Courville. Unsupervised learning of dense visual representations. In *NeurIPS*, 2020.
- [42] J. Pont-Tuset, F. Perazzi, S. Caelles, P. Arbeláez, A. Sorkine-Hornung, and L. Van Gool. The 2017 DAVIS challenge on video object segmentation. *arXiv:1704.00675 [cs.CV]*, 2017.
- [43] R. Ranftl, A. Bochkovskiy, and V. Koltun. Vision transformers for dense prediction. In *ICCV*, 2021.
- [44] J. Shi and J. Malik. Motion segmentation and tracking using normalized cuts. In *ICCV*, 1998.
- [45] J. Son. Contrastive learning for space-time correspondence via self-cycle consistency. In *CVPR*, 2022.
- [46] A. Stone, D. Maurer, A. Ayvaci, A. Angelova, and R. Jonschkowski. SMURF: self-teaching multi-frame unsupervised RAFT with full-image warping. In *CVPR*, 2021.
- [47] D. Sun, X. Yang, M. Liu, and J. Kautz. PWC-Net: CNNs for optical flow using pyramid, warping, and cost volume. In *CVPR*, 2018.
- [48] A. Tarvainen and H. Valpola. Mean teachers are better role models: Weight-averaged consistency targets improve semi-supervised deep learning results. In *NIPS*, 2017.
- [49] Z. Teed and J. Deng. RAFT: Recurrent all-pairs field transforms for optical flow. In *ECCV*, 2020.

- [50] Z. Tong, Y. Song, J. Wang, and L. Wang. VideoMAE: Masked autoencoders are data-efficient learners for self-supervised video pre-training. In *NeurIPS*, 2022.
- [51] C. Vondrick, A. Shrivastava, A. Fathi, S. Guadarrama, and K. Murphy. Tracking emerges by colorizing videos. In *ECCV*, 2018.
- [52] N. Wang, W. Zhou, and H. Li. Contrastive transformation for self-supervised correspondence learning. In *AAAI*, 2021.
- [53] X. Wang, A. Jabri, and A. A. Efros. Learning correspondence from the cycle-consistency of time. In *CVPR*, 2019.
- [54] Y. Wang, L. Lipson, and J. Deng. SEA-RAFT: Simple, efficient, accurate RAFT for optical flow. In *ECCV*, 2024.
- [55] J. Xu and X. Wang. Rethinking self-supervised correspondence learning: A video frame-level similarity perspective. In *ICCV*, 2021.
- [56] N. Xu, L. Yang, Y. Fan, D. Yue, Y. Liang, J. Yang, and T. S. Huang. YouTube-VOS: A large-scale video object segmentation benchmark. *arXiv:1809.03327 [cs.CV]*, 2018.
- [57] J. Zbontar, L. Jing, I. Misra, Y. LeCun, and S. Deny. Barlow Twins: Self-supervised learning via redundancy reduction. In *ICML*, 2021.
- [58] L. Zelnik-Manor and M. Irani. Degeneracies, dependencies and their implications in multi-body and multi-sequence factorizations. In *CVPR*, 2003.

A Qualitative Examples

Our supplemental material (.zip, 90MB) is accompanied by a qualitative video comparison. We select multiple validation sequences from DAVIS-2017 [42] and run linear probing using DINO2-S14 [39] as the baseline encoder.

- `a_vos_featup.mp4` compares FlowFeat against FeatUp [16]. The videos also visualise the ground-truth segmentation masks and the first three principal components of FlowFeat representation. FlowFeat achieves compelling segmentation accuracy, remains sharp at object boundaries and more temporally stable than FeatUp.
- `b_pca_featup.mp4` inspects the first three principal components of FlowFeat and FeatUp for two input resolutions: 224×400 and 480×854 . We observe that FlowFeat scales gracefully and reveals a greater level of detail. By contrast, FeatUp struggles to adapt to the higher resolution and exhibits static artefacts. Note that both FlowFeat and FeatUp were trained on 224×224 image crops.
- `c_pca_video_models.mp4` compares FlowFeat to VideoMAE [50] based on ViT-B16 and V-JEPA [5] based on ViT-L16, which are pre-trained on videos in a self-supervised manner. We observe that neither of these two models is capable of producing a satisfying level of granularity in the feature maps. Additionally, V-JEPA exhibits peculiar artefacts, which make it unsuitable for downstream dense tasks. In contrast, FlowFeat leverages video datasets more effectively, producing fine-grained and temporally stable feature representations.
- Finally, `d_pca_vs_loftup.mp4` compares FlowFeat to a concurrent work, LoftUp [21], *pre-trained with mask supervision* via the Segment Anything model [26]. LoftUp offers an improved representation over FeatUp and exhibits a high discrimination level of the background regions. However, LoftUp suffers from artefacts, often producing ragged-looking boundaries of moving objects and background elements. Without relying on mask annotation, FlowFeat demonstrates consistent spatial and temporal precision when it comes to dynamic objects. For example, observe sharper boundaries in the “goat” sequence, and a more distinguishable representation of the car and the dancers. These observations explain the quantitative advantage of FlowFeat over LoftUp on the VOS benchmark (*cf.* Tab. 1).

B Further Implementation Details and Analyses

B.1 Video object segmentation

Linear Probing. Linear probing maps the learned representations to object masks. The linear layer has $(d + 1) \times (C + 1)$ parameters, accounting for the bias term and the background class. The training process of the linear probe is standardised across all evaluated methods. Using the cross-entropy loss, we employ the Adam solver [25] and train the linear projection for 500 iterations with a learning rate of 5×10^{-3} and a weight decay of 5×10^{-4} . We run inference and training of the linear probe by fixing the image height at $480p$ and adjusting the width to be divisible by 64, as done by Caron et al. [9]. We apply linear probing on the native feature resolution produced by the model. If necessary, we resize the predicted masks to the original image resolution to compute the metrics w.r.t. the original ground truth masks.

Both FlowFeat and FeatUp [16] utilise a two-stage architecture: a pre-trained encoder that produces low-resolution features, followed by a decoder that generates high-resolution representations. To evaluate the contribution of the high-resolution features, we combine them with the encoder’s low-resolution feature map. In detail, we bilinearly upsample the backbone features and concatenate them with the high-resolution feature tensors. The linear layer projects this joint feature representation to the segmentation logits for each pixel.

Note that linear probing is not auto-regressive – in contrast to local KNN. Specifically, we run inference with the same pre-trained linear projection on all remaining frames in the video. Intuitively, linear probing in the context of VOS is akin to few-shot learning, and provides a more interpretable measure of the spatio-temporal representation quality.

To assess whether the improved VOS performance of FlowFeat is due to the higher feature resolution alone, we downsample the output features of FlowFeat and FeatUp to the same resolution as the

Table 5: **(a) Effect of reduced feature resolution in linear probing (DAVIS-2017, val)**. All features are downsampled to match the baseline encoder resolution. Δ indicates the absolute change in the VOS accuracy w.r.t. the original full-resolution setting of each model. Despite the lower resolution, FlowFeat retains strong VOS performance, confirming that high resolution alone does not explain the observed benefits; FlowFeat embeds a motion-based feature modality that is complementary to the encoder’s representation. **(b) FlowFeat generalizes to larger backbones (DAVIS-2017, val)**. As expected, training FlowFeat with ViT-L leads to a consistent improvement of VOS accuracy over the baseline – both for MAE and DINOv2.

(a)							(b)			
Method	Scale	$\mathcal{J}\mathcal{F}_m$	\mathcal{J}_m	\mathcal{F}_m	Δ	Δ	Method	$\mathcal{J}\mathcal{F}_m$	\mathcal{J}_m	\mathcal{F}_m
DINO2-S14 [39]	–	57.5	–	54.2	–	60.7	DINOv2-L14 [39]	59.4	55.8	63.0
+ FeatUp [16]	↓x14	59.5	-1.0	56.4	-1.0	62.6	+ FlowFeat-YT	66.9	63.4	70.4
+ FlowFeat-YT	↓x14	62.2	-3.6	58.2	-3.8	66.3	MAE-L14 [19]	46.7	44.4	49.0
+ FlowFeat-K	↓x14	62.3	-2.3	58.1	-2.9	66.4	+ FlowFeat-YT	55.4	52.0	58.9

Table 6: **Scaling up the feature resolution in local KNN probing (DAVIS-2017, val)**. We increase the feature resolution by a factor of two and re-run the local KNN unchanged otherwise. The Δ reports the absolute difference in the corresponding metric w.r.t. the base setting of local KNN. CRW [22] is a CNN-based approach provided for a reference. The encoder and FeatUp do not benefit from the higher feature resolution. By contrast, FlowFeat considerably improves its VOS accuracy.

Method	Scale	$\mathcal{J}\mathcal{F}_m$	\mathcal{J}_m	\mathcal{F}_m	Δ	Δ	Δ
CRW-Res18 [22]	×2	65.2	63.1	67.3			
DINO2-S14 [39]	×2	63.3	-1.8	62.8	-0.9	63.7	-2.9
+ FeatUp [16]	×2	64.6	-0.9	64.5	-0.5	64.6	-1.5
+ FlowFeat-YT	×2	70.3	+2.7	68.0	+2.4	72.5	+2.9
+ FlowFeat-K	×2	70.0	+1.5	67.5	+1.4	72.5	+1.6

baseline encoder (DINO2-S14 [39]). This enables us to directly compare the models under the identical conditions of the feature resolution. Tab. 5a reports the results. While all methods experience some drop in performance – as expected – both FlowFeat variants significantly outperform the baseline and FeatUp. This result demonstrates that FlowFeat yields accuracy gains not merely due to the higher resolution, but also due to the complementary properties derived from motion, which the encoder’s representation lacks.

To evaluate generalization of FlowFeat to the backbone architectures with larger capacity, we consider ViT-L and train FlowFeat by bootstrapping it from DINO2-L14 [39] and MAE-L14 [19]. We evaluate the models using the same linear probing protocol on VOS. As shown in Tab. 5b, FlowFeat leads to substantial performance gains for both models. These results confirm that FlowFeat is effective across different encoder architectures, with varying model capacities and pre-training schemes.

Local KNN. We adopt the label propagation approach from Caron et al. [9]. This protocol requires downsampling the high-resolution feature maps to match the encoder feature resolution. We apply label propagation independently on both the backbone and the downsampled features, and compute the mean of the resulting logits. This ensures hyperparameter consistency of our local KNN evaluation with previous work and across model architectures.

Since downsampling the high-resolution features goes against our motivation, we analyse the impact of the increased feature resolution in Tab. 6. Here, we keep the hyperparameters of the local KNN from the base setting above, but increase the resolution of the feature maps by a factor of 2. As a reference, we provide the VOS accuracy of CRW [22], a CNN-based approach producing the feature maps at the required resolution. Surprisingly, neither the encoder nor FeatUp benefit from the resolution increase. By contrast, FlowFeat improves the results further by significant margins and substantially outperforms the CNN-based reference.

Table 7: **Computational and runtime complexity.** We compare the total and decoder-only floating-point operations (FLOPs), as well as the throughput measured by the frames per second (FPS) rate. Here, we use the DINO2-S14 [39] baseline, the input resolution of 224×224 and RTX 8000 GPU.

Method	Total FLOPs	Decoder FLOPs	FPS
DINO2-S14 [39]	6.14B	–	176.79
+ FeatUp [16]	16.54B	10.33B	25.12
+ FlowFeat	23.43B	17.3B	105.82

B.2 Semantic segmentation

We keep the DPT decoder in FlowFeat frozen and only train a shallow, one-layer probe. For the low-resolution encoder features and the high-dimensional FeatUp representation we use linear probing. For FlowFeat, we complement the predictions from the encoder with the predictions provided by attention probing. Our implementation of attention probing is inspired by previous work [5]. In our evaluation, we extend this technique to dense prediction tasks. We initialise $C = 27$ (the number of semantic categories) learnable queries in the probe. Each query has the dimensionality of d , matching that of FlowFeat. We use a single block of cross-attention to condition the queries on the FlowFeat representation. Finally, we compute the dot product of the conditioned queries with the spatial feature grid produced by FlowFeat. As a result, we obtain a prediction of size $C \times H \times W$. We also found that downsampling the FlowFeat maps in the cross-attention block significantly improves the probe efficiency without detriment to the probing accuracy.

We train the models with Adam [25] using the cross-entropy loss. We sample mini-batches of size 32, setting the learning rate to 10^{-4} and weight decay to 0.001. All models tend to converge within 100K iterations, which takes less than a day on a single GPU – except for FeatUp, which runs longer, as we discuss in the next section.

For the post-hoc refinement (the “++” variants of FlowFeat), we use a simplified PAMR implementation [1]. Specifically, we use a single kernel of size 11×11 and a fixed scaling factor of 0.1 to produce the local affinity distribution. Crucially, we do not leverage the image intensities to compute the distribution, but replace it with the FlowFeat representation. The refinement runs for 10 steps.

B.3 Monocular depth estimation

The experiments on monocular depth largely follow the setting of the semantic segmentation above. The only conceptual difference is the definition of C , which in monocular depth stands for the number of depth bins. Specifically, to predict the AdaBins [6] representation with $C = 256$ bins (*i.e.* a tensor of size $C \times H \times W$), we initialise $C = 256$ learnable queries in the probe and pass them through a single block of cross-attention. As in semantic segmentation, we compute the dot product of the conditioned queries with the FlowFeat tensor. We train the probes with Adam optimizer [25], batch size 16 and set the learning rate to 10^{-4} and weight decay to 10^{-5} . Following previous work [4, A.3.1], we use a combination of the scale-invariant depth loss [13] and the gradient matching loss [30]. We train all models for up to 100K iterations.

C Efficiency Analysis

We analyse the computational and runtime efficiency of FlowFeat and compare those to the baseline encoder DINO2-S14 [39] and FeatUp [16]. Specifically, we set the input resolution to 224×224 and measure floating-point operations (FLOPs) as well as the FPS rate on an RTX 8000 GPU with 48GB of memory. Tab. 7 summarises the benchmark results. In fact, FlowFeat incurs more FLOPs in total than FeatUp. However, all operations in the DPT decoder of FlowFeat are highly parallelisable, hence efficient. As a result, FlowFeat achieves a significantly higher throughput. In the practical terms of FPS, FlowFeat runs four times faster than FeatUp. Indeed, FeatUp’s implementation of the bilateral upsampler, though impressively more efficient than previous work, still falls short of the DPT runtime efficiency.

D License note

The parts of the code we use from Jabri et al. [22] (the label propagation algorithm) are released under a MIT license. The datasets YouTube-VOS, Kinetics-400 are licensed under the Creative Commons Attribution 4.0 International License, while DAVIS-2017 is provided under the Creative Commons Attribution-NonCommercial 4.0 International License.